Physica Scripta

PAPER

Simulation of UV VCSEL with Grad AlGaN to improve output power and current spreading at high current

To cite this article: Zhi-Jie Zou *et al* 2026 *Phys. Scr.* **101** 075904

Physica Scripta

RECEIVED
9 December 2025

REVISED
15 January 2026

ACCEPTED FOR PUBLICATION
3 February 2026

PUBLISHED
12 February 2026

PAPER

Simulation of UV VCSEL with Grad AlGaN to improve output power and current spreading at high current

Zhi-Jie Zou[1], **Bing An**[1], **Yu-Kun Wang**[1], **Ya-Chao Wang**[1], **Yang Mei**[1,*] **and Bao-Ping Zhang**[1,2,*]

[1] Department of Microelectronics and Integrated Circuits, Xiamen University, Xiamen 361005, People's Republic of China
[2] Institute of Nanoscience and Applications (INA), Southern University of Science and Technology (SUSTech), Shenzhen 518055, People's Republic of China
[*] Authors to whom any correspondence should be addressed.

E-mail: meiyang@xmu.edu.cn and zhangbp@sustech.edu.cn

Keywords: UV VCSELs, current spreading layer, graded AlGaN insertion layer

Supplementary material for this article is available online

Abstract

Traditional UV VCSELs with ITO current spreading layer are limited by the large absorption loss of ITO in UV spectral region, which makes electrically pumped UV VCSELs hardly to lase. This study proposes an optimized structure for UV VCSEL containing a graded AlGaN insertion layer and a much thinner ITO layer (10 nm) to improve the lateral current spreading and light output power. After the insertion of the graded AlGaN layer, the carrier concentration in the p-GaN region was significantly increased, which not only improved carrier injection efficiency but also reduced the voltage consumption in the p-GaN region, thereby decreasing the series resistance of the device. Simulation results show that UV VCSELs with the Grad AlGaN insertion layer exhibit significantly improved current spreading performance at high current. Compared with the traditional structure using 10 nm ITO current spreading layer, the light output power was increased from 0.85 to 1.34 mW at 20 mA, with an increasement by 57.7% and the series resistance was reduced from 101 to 51 Ω by 49.5%. On the other hand, the threshold current was slightly increased from 1.74 to 2.14 mA by 18.9% as a compromise.

1. Introduction

Vertical-cavity surface-emitting lasers (VCSELs) have attracted significant attention due to their low threshold current, single longitudinal mode output, high coupling efficiency with optical fibers, and ease of integration into two-dimensional arrays [1–3]. Since GaN-based ultraviolet (UV) LEDs have been widely used in applications such as UV curing, skin treatment, sterilization, and UV communication, UV VCSELs, which offer advantages such as smaller size, better coherence, and focused beams, are expected to have even greater potential in various applications [4]. However, the development of UV VCSELs has faced many challenges. Particularly, UV VCSELs are mainly achieved by optical pumping at present, and electrically injected UV VCSELs are hindered by difficulties including structural design, epitaxial growth, and device fabrication processes. Among these challenges, the strong absorption of UV light by the current spreading layer ITO (indium tin oxide) diminishes the emission intensity generated from the active region and prevents the occurrence of lasing. Thus, the optical absorption loss in ITO layer is an important issue that needs to be severely considered.

Blue and green GaN-based VCSELs typically use a 20–30 nm thick ITO layer to act as the current spreading layer [5]. However, this solution is not suitable for UV VCSELs due to the relatively high absorption of ITO in the UV wavelength range. Lai and Konig *et al* carefully measured the absorption characteristics of ITO over different spectral ranges, revealing a significant increase in the absorption coefficient of ITO in the UV wavelength range, which varies from 3200 cm^{-1} to 4000 cm^{-1} in the wavelength range from 400 nm to 390 nm [6–8]. To address this issue, researchers have proposed various optimization designs. Zheng *et al* abandoned

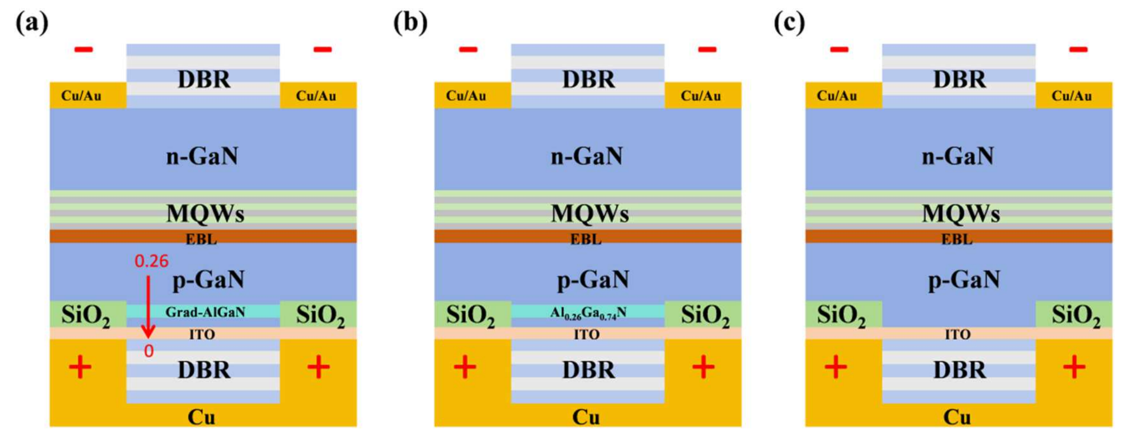

Figure 1. Structure diagrams of (a) G-VCSEL, (b) F-VCSEL and (c) Normal VCSEL.

the ITO layer and used a periodic AlGaN/GaN structure, leveraging the 2DHG/2DEG generated at the interfaces to improve the lateral current spreading capability [9]. The application of AlGaN-based tunnel junctions (TJ) has also demonstrated significant potential for their use in electrically injected UV VCSELs [10–14]. The TJ VCSEL, as developed by Leonard *et al*, demonstrates a remarkable 324% improvement in differential efficiency and a 56% reduction in threshold current density compared to the ITO VCSEL [14]. These studies focus on finding new current spreading structures that can completely replace ITO, however, new issues are introduced to the device. The current spreading layer of the periodic AlGaN/GaN structure can lead to snapback effect, and turn-on voltage and series resistance of device are increased [9]. The introduction of tunnel junctions also increases the turn-on voltage and series resistance of the device [15]. Thinning the ITO layer is another method to reduce light absorption loss. Studies by An *et al* shows that thinning ITO from 30 nm to 20 nm can reduce light absorption loss and increase light output power, but it also increases the series resistance of device [16]. The experimental results by Mazur *et al* show that the sheet resistance increases significantly as the ITO thickness is reduced from 30 nm to 10 nm [17]. Therefore, new strategies need to be developed to obtain current spreading structures with both small sheet resistance and optical absorption simultaneously.

In this study, an AlGaN layer with graded Al composition (0.26–0 along growth direction) was designed to insert into the p-GaN layer to enhance the current spreading and carrier injection efficiency into the active region, and the performances of the devices were simulated by using the commercial simulation software Crosslight PICS3D. The device performances of normal VCSEL without AlGaN insertion layer and VCSEL with a concentration fixed AlGaN insertion layer were also simulated for comparation. For all device structures, a thin ITO layer of 10 nm was used in the simulation model. Simulation results show that the insertion of the graded AlGaN layer strengthens the polarization electric field at the edge of the p-GaN region, leading to the accumulation of more electron–hole pairs at the p-GaN/AlGaN boundary. These carriers generate a shielding electric field which is opposite to the applied external field, significantly reducing the total electric field in the central region of the p-GaN. Compared with the fixed AlGaN insertion layer, inserting a graded AlGaN leads to much higher carrier density within the p-GaN layer. This can enhancing shielding electric field of p-GaN. Meanwhile, the polarization induced doping in the continuously graded AlGaN layer leads to a movable three-dimensional hole gas (3DHG) [18, 19]. As a result, the carrier concentration in the central region of the p-GaN increases substantially and hole vertical injection to the active region is improved. On the other hand, the electron barrier of the gradual AlGaN insertion layer further prevents electron leakage from the active region. Compared to the normal UV VCSEL with a 10 nm ITO layer, the VCSEL with graded AlGaN insertion layer shows an increase of the output power from 0.85 to 1.34 mW by 57.7% and decrease of the series resistance from 101 to 51 Ω by 49.5%, but the threshold current was increased from 1.74 to 2.14 mA by 18.9% as a compromise.

2. Simulation model

Figure 1 presents the schematical structure of the three different VCSELs. The F-VCSEL added a 30 nm $Al_{0.26}Ga_{0.74}N$ insertion layer with fixed Al concentration into p-GaN based on the Normal VCSEL structure, while the G-VCSEL incorporates a 30 nm graded AlGaN insertion layer (Al content decreased from 0.26 to 0 along growth direction). To reduce absorption losses from the ITO, all three structures employ a very thin ITO layer of 10 nm. The basic model of the device consists of p-GaN with a doping concentration of 5×10^{17} cm^{-3}, 3

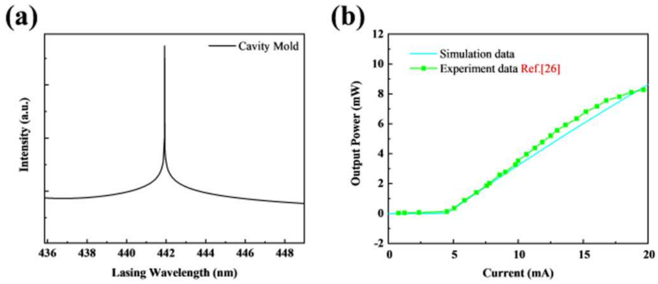

Figure 2. (a) Spectrum of cavity mode at 20 mA; (b) PI characteristic curves for experiment and simulation [26].

Table 1. Detailed parameters of the G-VCSEL.

	Material	Thickness(nm)	Doping concentration(cm^{-3})
n-DBR	HfO_2/SiO_2	(51/67)*20 pairs 2360	—
n-GaN	GaN	530	n:5e18
MQW	$In_{0.08}Ga_{0.92}N/GaN$	(2.2/4)*3 pairs	
EBL	$Al_{0.2}Ga_{0.8}N$	20	p:3e17
n-GaN	GaN	129	p:5e17
Graded p-AlGaN	AlGaN(0.26–0)	30	p:5e17
Passivated region	SiO_2	50	—
Current Spreading layer	ITO	10	—
Optical adjustment layer	HfO_2	40.4	—
p-DBR	HfO_2/SiO_2	(51/67)*10 pairs 1180	—

pairs of $In_{0.08}Ga_{0.92}N/GaN$ quantum well active region, an $Al_{0.2}Ga_{0.8}N$ EBL with a doping concentration of 3×10^{17} cm^{-3}, n-GaN with doping concentration of 5×10^{18} cm^{-3}, and an ITO current spreading layer. The diameter of the current confinement aperture is 2.5 μm, and the lasing wavelength of the devices is 396.8 nm. Other device parameters are detailed in table 1.

The commercial software Crosslight PICS3D employs crucial physical modeling. Typical equations include the Schrödinger equation, Poisson equation, drift-diffusion equation, and others. The Shockley-Read-Hall (SRH) lifetime is set to 1×10^{-8} s, and the Auger recombination coefficient is set to 1.4×10^{-31} cm^6s^{-1} to account for Auger recombination in the material [20, 21]. The conduction band/valence band offset ratio in the multi-quantum well is set to 70:30 [22]. The average optical background loss in the cavity, excluding ITO, is set to 10 cm^{-1} [23], and the optical absorption loss coefficient of ITO is set to 4000 cm^{-1} [24]. The polarization level is set to 40% to approximate the polarization charges at the interface [25]. The current-induced thermal effect was not included in the simulation model.

To verify the accuracy of the simulation model, we simulated the VCSEL experimental device with a lasing wavelength of 442 nm by Kuramoto *et al* [26]. Figure 2(a) shows spectrum of cavity mode (442 nm) at 20 mA. As shown in figure 2(b), the experimental and simulated PI (output power versus current) curves are consistent. Table 2 lists the key materials and parameters used in the experiment and simulation. The current-limiting aperture is 8 μm, and the cavity length is 5 λ.

3. Results and discussion

Figure 3 shows the simulated PI curves of the three different VCSELs. The optical output power of the G-VCSEL at 20 mA is 1.34 mW, which is 57.65% higher than the Normal VCSEL, and 77.72% higher than the F-VCSEL. In addition, as shown in the inset of figure 3, the threshold current of the G-VCSEL is 2.14 mA, which is decreased by 18.94% compared to the F-VCSEL, and increased by 19.21% compared to the Normal VCSEL. A parameter sensitivity study was also conducted by varying the polarization strength, SRH lifetime, Auger coefficient, and optical loss values used in the simulation model (Supplementary Information, tables S1–S4). The simulation model of this study and the optimization of output by introducing graded AlGaN insertion layer is proved robust under different simulation parameters. To further understand the change of device performance, energy band structures of the three VCSELs under different current were systemically analyzed. The energy band of GaN based devices can be modulated by the polarization effect. As seen in figure 4(a), the spontaneous polarization (P_{sp}) direction of the Ga polar p-GaN and AlGaN is opposite to the epitaxial growth

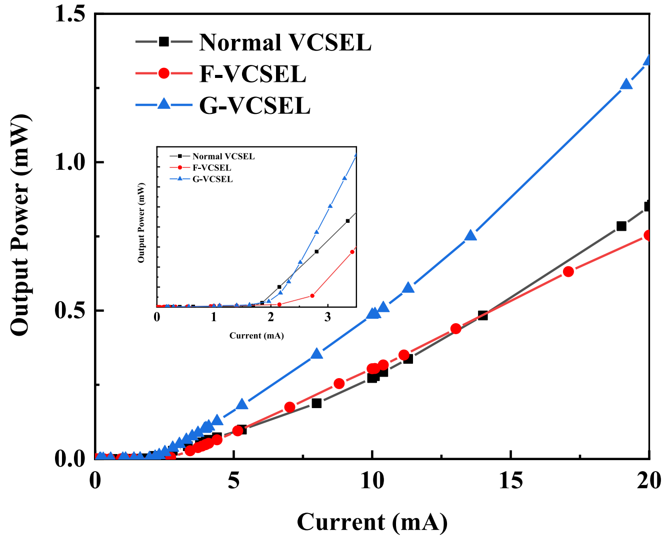

Figure 3. PI characteristic curves of three types VCSEL. Inset is an enlarged figure at lower currents.

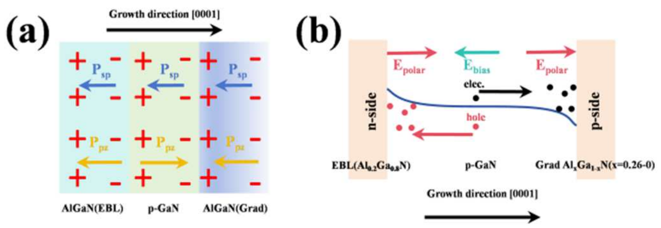

Figure 4. (a) P_{SP} and P_{PE} of p-GaN and AlGaN in [0001] growth direction; (b) simplified diagram of electric field and energy band in [0001] growth direction.

Table 2. Detailed physical parameters of simulation and experiment [26].

	Material	Experiment (nm)	Simulation (nm)
p-DBR	Nb_2O_5/SiO_2	10.5 pairs	10.5 pairs
Current spreading layer	ITO	20	20
Passivated region	SiO_2	20	20
p-GaN	GaN	void	84
EBL	p-AlGaN	20	20
MQW	InGaN/GaN	39	39
n-GaN	GaN	660	680
n-DBR	AlInN/GaN	42 pairs	42 pairs

direction [0001]. The piezoelectric polarization (P_{pz}) direction of AlGaN is also opposite to the growth direction, while the P_{pz} direction in the p-GaN region aligns with the growth direction. This is because the lattice constant of AlGaN is smaller than that of GaN, resulting in compressive stress in the p-GaN region, which causes the P_{pz} in p-GaN to be opposite to P_{sp}. The schematical band tilt of p-GaN after the insertion of AlGaN layer is shown in figure 4(b). The energy band of p-GaN near the interface of p-GaN/EBL and p-GaN/AlGaN insertion layer exhibit significant bending due to the total polarization electric field (E_{polar}), which is opposite to the growth direction. The combined effect of the bias electric field (E_{bias}) and the E_{polar} at the p-GaN edge causes holes to accumulate near the EBL edge, while electrons accumulate near the graded AlGaN edge. This results in the formation of a carrier shield electric field (E_{shield}) at the center of the p-GaN layer, which shields the E_{bias}, leading to the flattening of the energy bands at the center of the p-GaN region.

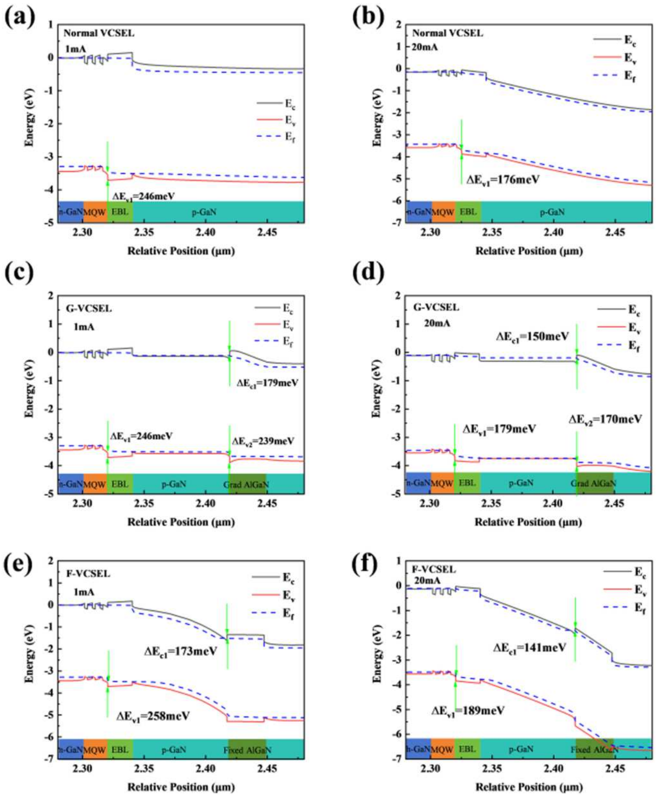

Figure 5. (a) Band diagram of Normal VCSEL at 1 mA; (b) Band diagram of Normal VCSEL at 20 mA; (c) Band diagram of G-VCSEL at 1 mA; (d) Band diagram of G-VCSEL at 20 mA; (e) Band diagram of F-VCSEL at 1 mA; (f) Band diagram of F-VCSEL at 20 mA. ΔE_{c1} was used to evaluate the electron barrier caused by graded AlGaN and ΔE_{v1} was used to evaluate the hole injection barrier caused by EBL.

The calculated energy band of the three VCSELs under different current before (1 mA) and after lasing (20 mA) are shown in figure 5. Typically, the AlGaN EBL can block the electron leakage from the active region, but it will also introduce a barrier for the hole injection from p-GaN to the active region. The energy offset between hole quasi-Fermi level and valance band of EBL ΔE_{v1} was used to evaluate the hole injection barrier caused by EBL. The ΔE_{v1} in the G-VCSEL is similar to that in the Normal VCSEL and F-VCSEL for both low and high current. However, the electron and hole quasi-Fermi level is closer to the valance and conduction band in the p-GaN layer between the EBL and the inserted graded AlGaN in G-VCSEL when compared to that of the Normal VCSEL and F-VCSEL, which means a much higher carrier density in the p-GaN layer. Therefore, with nearly the same ΔE_{v1}, the hole injection to the active region is more efficient and the sheet resistant of p-GaN is smaller in G-VCSEL. Figures 5(c) and (d) show that the graded AlGaN creates an additional electron barrier (ΔE_{c1}), which is 150 meV at 20 mA and 179 meV at 1 mA, compared to the Normal VCSEL. This additional electron barrier helps prevent electron leakage from the p-GaN region. It is noted that, compared with the Normal VCSEL, the graded AlGaN also introduces an additional hole injection barrier ΔE_{v2} along [000–1] direction from AlGaN insertion layer to p-GaN,, which is 170 meV at 20 mA and 239 meV at 1 mA. This additional hole barrier can be the reason of the slight higher threshold current of G-VCSEL than the N-VCSEL under small injected current. Detailed value of ΔE_{c1}, ΔE_{v1} and ΔE_{v2} for G-VCSEL, F-VCSEL and Normal VCSEL at different currents are shown in table 3.

Figure 6 shows the hole density distribution in the active region, p-GaN, and AlGaN insertion layer for the three VCSELs with different structures. Compared with the F-VCSEL, inserting a graded AlGaN in the G-VCSEL leads to much higher carrier density within the p-GaN layer. This can be attributed to the polarization induced doping in the continuously graded AlGaN layer, which leads to a movable three-dimensional hole gas (3DHG) [18, 19]. This favors more holes to be injected from the graded AlGaN into the p-GaN region, thereby improving the efficiency of hole vertical injection into the active region. Compared with the Normal and G-VCSEL, the energy band of p-GaN in F-VCSEL is more tilted, as shown in figures 5(e) and (f). This is because the hole density in the inserted AlGaN layer is much lower, and the energy barrier hinders hole injection into the p-GaN, leading to an increased series resistance in the p-GaN. Under the same injection current, the electric potential difference across the p-GaN increases, resulting in pronounced band bending.

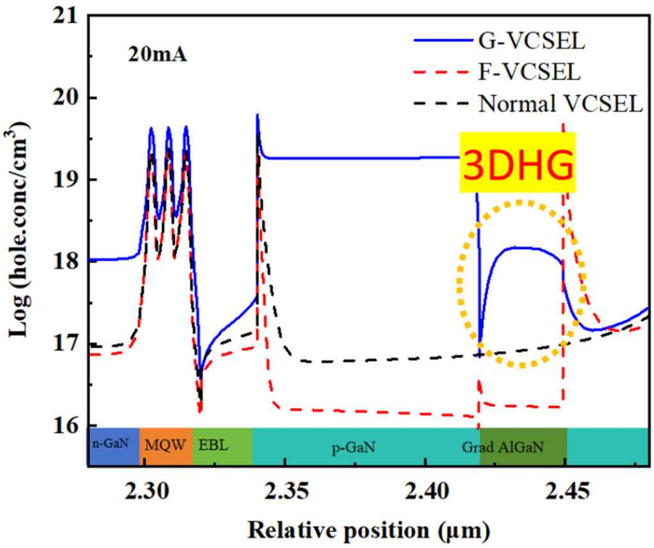

Figure 6. Comparison of hole concentration at 20 mA.

Table 3. Simulated potential barriers of electrons and holes in G-VCSEL, F-VCSEL and Normal VCSEL.

	Current	ΔE_{c1}	ΔE_{v1}	ΔE_{v2}
G-VCSEL	1 mA	179 meV	246 meV	239 meV
	20 mA	150 meV	179 meV	170 meV
F-VCSEL	1 mA	173 meV	258 meV	—
	20 mA	141 meV	189 meV	—
Normal VCSEL	1 mA	—	246 meV	—
	20 mA	—	176 meV	—

The detailed electron and hole density inside the active region of the three VCSELs under 1 and 20 mA are shown in figure 7. The electron concentration in the quantum wells of the G-VCSEL and F-VCSEL are higher compared to the Normal VCSEL, as illustrated in figures 7(a) and (b). Because the electron mobility is much higher than that of holes which causes electrons to accumulate in the first quantum well near the p-side, the electron concentration is the highest in the first quantum well near the p-side. The additional electron barrier ΔE_{c1} caused by the AlGaN insertion layer can be the reason of the higher electron density in the active region of G-VCSEL and F-VCSEL. Under low current of 1 mA (before lasing), the hole concentration in the quantum wells of G-VCSEL and Normal VCSEL does not differ significantly, while the hole concentration in F-VCSEL is notably lower, as shown in figure 7(c). This can be caused by the smaller hole concentration in p-GaN and AlGaN insertion layer, as well as the hole injection barrier caused by the fixed AlGaN insertion layer. Generally, the carrier concentration in the active region of G-VCSEL is higher than other structures, especially under high current. The high current not only enhances the carrier screening effect in the p-GaN between EBL and graded AlGaN, but also reduces the hole barrier in graded AlGaN. Thus, significantly more holes are injected into active region in G-VCSEL, compared with Normal VCSEL at 20 mA. The higher carrier density in the active region leads to an increase of radiative recombination rate and stimulated radiative recombination rate of the device, as shown in figures 7(e) and (f). Based on the above discussion, it is clear that the graded AlGaN structure enhances the vertical hole injection on the positive side. Moreover, on the negative side, an additional hole injection barrier ΔE_{v2} is newly introduced. Both factors influence the hole concentration in the active region and therefore determine the threshold gain of the G-VCSEL. At lower current near lasing, the enhanced hole concentration and mobility from the graded AlGaN polarization-induced doping is not enough to overcome the blocking effect of the graded AlGaN hole barrier, thereby inducing the slightly higher threshold current than Normal VCSEL.

Figure 8 shows I-V curves of the three VCSELs. The series resistance of G-VCSEL is calculated to be 51 Ω, better than 101 Ω of the Normal VCSEL and similar to 50 Ω of the normal structure VCSEL using 20 nm ITO, which was reported by Zheng *et al* [9]. The higher carrier density in active region and p-GaN of the G-VCSEL

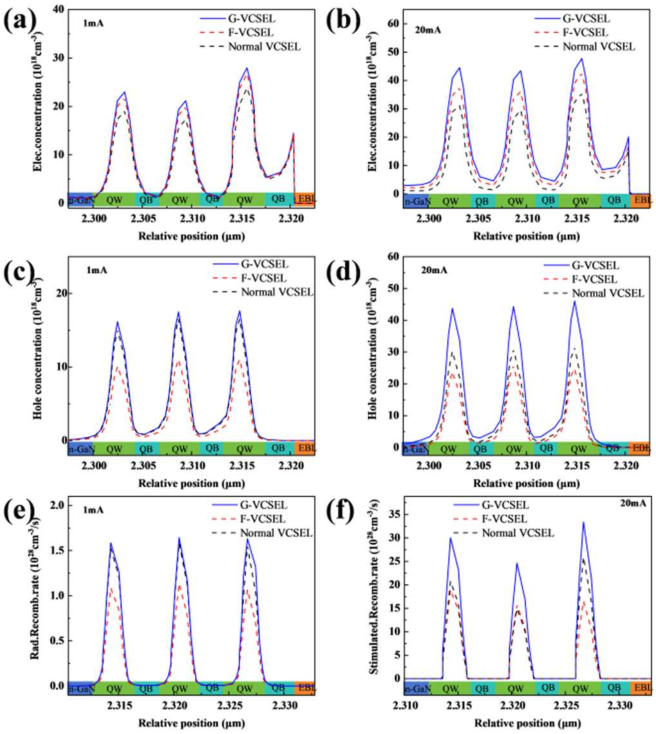

Figure 7. (a) Comparison of electron concentration in the active region at 1mA; (b) Comparison of electron concentration in the active region at 20 mA; (c) Comparison of hole concentration in the active region at 1 mA; (d) Comparison of hole concentration in the active region at 20 mA; (e) Radiative recombination rate in the active region at 1mA. (f) Stimulated radiative recombination rate in the active region at 20 mA.

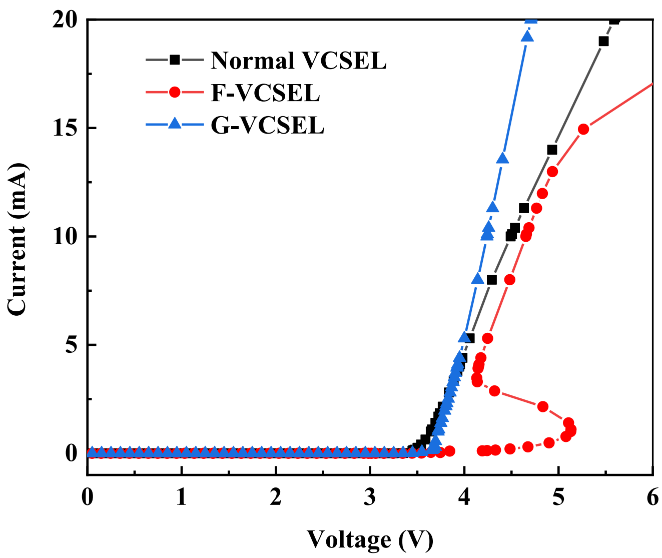

Figure 8. IV characteristic curves.

are essential to realize the smaller series resistance. In addition, the threshold voltage of G-VCSEL is 3.70 V, slightly worse than 3.59 V of the Normal VCSEL and 3.52 V of the normal structure with 20 nm ITO [9], which is due to the graded AlGaN barrier and thinner ITO.

It is worth noting that, at 4–5 V, the F-VCSEL exhibits snapback effect [9], where the current increases and voltage decreases significantly once the voltage exceeds the threshold voltage(5.2 V). This is due to the fact that, before the threshold, carriers hardly overcome the fixed AlGaN barrier, resulting in increasing series resistance. After the threshold, large number of carriers accumulated on both sides of the AlGaN barrier can pass through, leading to significantly increasing current and decreasing voltage in the p-GaN between EBL and fixed AlGaN layer. As the current increases from 1 mA to 4 mA, the electrical potential of the p-GaN layer decreases from

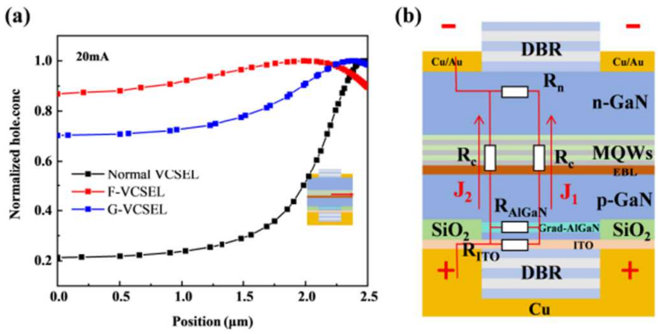

Figure 9. (a) Normalized lateral hole concentration inside the first quantum well near the p-GaN side of Normal VCSEL, F-VCSEL and G-VCSEL at 20 mA; (b) Equivalent current diagram of G-VCSEL.

1.74 V to 0.70 V, resulting in a negative slope of the IV curve. This abrupt change could potentially lead to device burnout and should be avoided. G-VCSEL addresses this issue by setting an appropriate gradual Al composition gradient and adjusting the thickness of the AlGaN layer.

The homogeneity of lateral hole distribution inside the active region can be used to assess the device's current extension capability in the p-side region [9, 16]. The Normalized lateral hole distribution, which is the normalization of the maximum hole concentration in the three devices themselves, inside the first quantum well near the p-GaN side of the three VCSELs under 20 mA were extracted, as shown in figure 9(a). The current extension of the G-VCSEL outperforms the Normal VCSEL, but not as good as the F-VCSEL. The difference of the current spreading ability of the three VCSELs can be simply analyzed by the current density ratio J2/J1 as defined by the following equation [9, 16]:

$$\frac{J_2}{J_1} = 1 + \frac{R_{parallel} + R_n}{R_c}$$

where J_1 and J_2 represent the current density at the center and edge of the current confinement aperture, respectively. R_{AlGaN}, R_{ITO} and R_n represent the lateral resistance of the AlGaN, ITO, and n-GaN, respectively. R_c represents the resistance of the resonant cavity in vertical direction. $R_{parallel}$ represent the parallel resistance of R_{AlGaN} and R_{ITO}. The equivalent circuit diagram of the G-VCSEL is shown in figure 9(b). The graded AlGaN in G-VCSEL has the higher hole mobility than p-doping GaN [27](Supplement information, 3), reducing the R_{AlGaN} and decreasing the ratio (J_2/J_1), which is beneficial in the lateral current spreading. However, due to the high carrier concentration in the p-GaN of G-VCSEL, the R_c is also reduced, increasing the ratio (J_2/J_1), which is beneficial for carrier injection efficiency and series resistance reduction but detrimental to the lateral current spreading. This is why the light output power of G-VCSEL significantly better than F-VCSEL, but the current extension capability is slightly insufficient at 20 mA. Reducing the R_{AlGaN} can be an effective method for further optimizing the lateral current spreading in G-VCSEL. Thus, as a compromise, compared with Normal VCSEL, G-VCSEL sacrifices the threshold current to improve the output power, the series resistance and the current spreading at high current. The overall performance is greatly improved.

The current-induced thermal effects in GaN based VCSELs are also important issues cannot be overlooked during device design and fabrication. The performance of G-VCSEL was calculated using simulation model incorporating current-induced thermal effects (Supplement information, figure S1). The PI curve of the G-VCSEL shows that the thermal rollover occurs at a high current of 56.7 mA. The maximum current of above discussion in this study is 20 mA, much smaller than the thermal rollover current. Therefore, the above conclusions about the optimization of device performance by the graded AlGaN insertion layer remain credible without considering thermal effect. Furthermore, the only difference among the three device structures is the thin AlGaN insertion layer, which has a negligible effect on the overall thermal resistance of the devices.

In terms of device fabrication feasibility, the graded Al composition layer requires precise control over the Al composition profile, which imposes stricter requirements on the stability of temperature and gas flow in the MOCVD chamber. In our previous work, we experimentally developed GaN based VCSELs with a graded AlGaN electron blocking layer with Al composition gradually decreasing from 0.2 to 0 along the [0001] direction [28]. The device performance was improved when compared with normal structures [28], thus demonstrating the practical feasibility of fabricating graded AlGaN layers. In addition, we have previously proposed an ITO-free approach for VCSELs, using AlGaN/GaN super-lattice structure as a substitute [9]. This approach avoids the absorption loss caused by ITO, but it also faces challenges such as the difficulty in growth of thin AlGaN/GaN super-lattice layers, the requirement of epitaxial regrowth, and a relatively higher threshold voltage compared with G-VCSEL.

4. Conclusion

In this study, a combined current spreading structure including a graded AlGaN insertion layer and 10 nm ITO layer was designed for GaN based VCSELs emitting in UV spectral region. The graded AlGaN insertion layer enhances carrier injection efficiency and lowers series resistance. Compared to the traditional VCSEL with 10 nm ITO current spreading layer, the light output power was increased by 57.7% at 20 mA and the series resistance was reduced by 49.5%, but the threshold current was increased by 18.9% as the trade-off. Compared with the ITO-free structure [9], this work is expected to provide a simple method to improve the device overall performance of GaN based VCSELs in UV spectral region.

Acknowledgments

This work was supported by the National Natural Science Foundation of China (62234011, 62474150, U21A20493), the National Key Research and Development Program of China (2024YFB3613100), the Shenzhen Science and Technology Program (ZDSYS20220527171201003), the Natural Science Foundation of Fujian Province (2023J05020), the Natural Science Foundation of Guangdong Province (2025A1515011349), the high level of special funds of SUSTech (G03034K002).

Data availability statement

All data that support the findings of this study are included within the article (and any supplementary files).

Author contributions

Zhi-Jie Zou 0009-0006-3076-1419
Conceptualization (equal), Data curation (equal), Formal analysis (equal), Methodology (equal), Software (equal), Writing – original draft (equal), Writing – review & editing (equal)

Bing An 0009-0000-1062-2055
Data curation (equal), Validation (equal)

Yu-Kun Wang
Investigation (equal), Visualization (equal)

Ya-Chao Wang 0009-0003-2770-6185
Formal analysis (equal), Writing – review & editing (equal)

Yang Mei 0000-0001-7190-0338
Supervision (equal), Validation (equal), Writing – review & editing (equal)

Bao-Ping Zhang
Funding acquisition (equal), Project administration (equal), Supervision (equal), Writing – review & editing (equal)

References

[1] Huang C Y, Hong K B, Huang Z T, Hsieh W H, Huang W H and Lu T C 2021 Challenges and advancement of blue III-nitride vertical-cavity surface-emitting lasers *Micromachines* **12** 19
[2] Xu H, Mei Y, Xu R B, Ying L Y, Su X L, Liu J P and Zhang B P 2020 Green VCSELs based on nitride semiconductors *Jpn. J. Appl. Phys.* **59** 9
[3] Yu H C, Zheng Z W, Mei Y, Xu R B, Liu J P, Yang H, Zhang B P, Lu T C and Kuo H C 2018 Progress and prospects of GaN-based VCSEL from near UV to green emission *Prog. Quantum Electron.* **57** 1–19
[4] Kneissl M and Rass J 2016 *III-Nitride Ultraviolet Emitters* (Springer) 227
[5] Ji K, Tian K and Gao Z H 2023 Lattice-matched AlInN/GaN bottom DBR impact on GaN-based vertical-cavity-surface-emitting laser diodes: systematical investigations *Appl. Optics* **62** 3431–8
[6] Lai F, Lin L, Gai R, Lin Y and Huang Z 2007 Determination of optical constants and thicknesses of In 2O 3:Sn films from transmittance data *Thin Solid Films* **515** 7387–92
[7] König T A F, Ledin P A, Kerszulis J, Mahmoud M A, El-Sayed M A, Reynolds J R and Tsukruk V V 2014 Electrically tunable plasmonic behavior of nanocube-polymer nanomaterials induced by a redox-active electrochromic polymer *Acs Nano* **8** 6182–92

[8] Mehta K, Liu Y-S, Wang J, Jeong H, Detchprohm T, Park Y J, Alugubelli S R, Wang S, Ponce F A and Shen S-C 2018 Lateral current spreading in III-N ultraviolet vertical-cavity surface-emitting lasers using modulation-doped short period superlattices *IEEE J. Quantum Electron.* **54** 1–7
[9] Zheng Z M, Wang Y K, Mei Y, Long H, Ying L Y, Zheng Z W and Zhang B P 2023 Current spreading structure of GaN-based vertical-cavity surface-emitting lasers *Opt. Lett.* **48** 5141–4
[10] Clinton E A, Engel Z, Vadiee E, Carpenter J V and Doolittle W A 2019 Ultra-wide-bandgap AlGaN homojunction tunnel diodes with negative differential resistance *Appl. Phys. Lett.* **115** 082104
[11] Kuhn C, Sulmoni L, Guttmann M, Glaab J, Susilo N, Wernicke T, Weyers M and Kneissl M 2019 MOVPE-grown AlGaN-based tunnel heterojunctions enabling fully transparent UVC LEDs *Photon. Res.* **7** B7–B11
[12] Zhang Y, Jamal-Eddine Z, Akyol F, Bajaj S, Johnson J M, Calderon G, Allerman A A, Moseley M W, Armstrong A M and Hwang J 2018 Tunnel-injected sub 290 nm ultra-violet light emitting diodes with 2.8% external quantum efficiency *Appl. Phys. Lett.* **112** 071107
[13] Malinverni M, Martin D and Grandjean N 2015 InGaN based micro light emitting diodes featuring a buried GaN tunnel junction *Appl. Phys. Lett.* **107** 051107
[14] Leonard J T, Young E C, Yonkee B P, Cohen D A, Margalith T, Denbaars S P, Speck J S and Nakamura S 2015 Demonstration of a III-nitride vertical-cavity surface-emitting laser with a III-nitride tunnel junction intracavity contact *Appl. Phys. Lett.* **107** 75–290
[15] Shen C C, Lu Y T, Yeh Y W, Chen C Y and Kuo H C 2019 Design and fabrication of the reliable GaN based vertical-cavity surface-emitting laser via tunnel junction *Crystals* **9** 187
[16] An B, Wang Y K, Wang Y C, Zou Z J, Mei Y, Long H, Zheng Z W and Zhang B P 2024 Structure design of UVA VCSEL for high wall plug efficiency and low threshold current *Photonics* **11** 13
[17] Mazur M, Pastuszek R, Wojcieszak D, Kaczmarek D and Lubanska A 2020 Effect of thickness on optoelectronic properties of ITO thin films *Circuit World Ahead-of-Print* **48** 149–59
[18] Zhang L, Ding K, Yan J C, Wang J X, Zeng Y P, Wei T B, Li Y Y, Sun B J, Duan R F and Li J M 2010 Three-dimensional hole gas induced by polarization in (0001)-oriented metal-face III-nitride structure *Appl. Phys. Lett.* **97** 252105
[19] Cao Y W, Lv Q J, Yang T P, Mi T T, Wang X W, Liu W and Liu J L 2023 Realization of high-efficiency AlGaN deep ultraviolet light-emitting diodes with polarization-induced doping of the p-AlGaN hole injection layer *Chin. Phys. B* **32** 7
[20] Hang S, Zhang Y, Gao Y, Qiu X and Zhang Z H 2020 On the origin for the hole confinement into apertures for GaN-based VCSELs with buried dielectric insulators *Opt. Express* **28** 8668–79
[21] Mackowiak P and Nakwaski W 2000 Designing guidelines for possible continuous-wave-operating nitride vertical-cavity surface-emitting lasers *J. Phys. D* **33** 642
[22] Zi-Hui, Zhang, Swee, Tiam, Tan, Zabu, Kyaw, Yun, Ji and Wei 2013 InGaN/GaN light-emitting diode with a polarization tunnel junction *Appl. Phys. Lett.* **102** 1028
[23] Mnatsakanov T T, Levinshtein M E, Pomortseva L I, Yurkov S N and Khan M A 2003 Carrier mobility model for GaN *Solid-State Electron.* **47** 111–5
[24] Minenkov A, Hollweger S, Duchoslav J, Erdene-Ochir O, Weise M, Ermilova E, Hertwig A and Schiek M 2024 Monitoring the electrochemical failure of indium tin oxide electrodes via operando ellipsometry complemented by electron microscopy and spectroscopy *ACS Appl. Mater. Interfaces* **16** 9517–31
[25] Qiu X, Zhang Y, Hang S, Gao Y, Kou J, Tian K, Zheng Q, Li Q and Zhang Z 2020 Enhancing the lateral current injection by modulating the doping type in the p-type hole injection layer for InGaN/GaN vertical cavity surface emitting lasers *Opt. Express* **28** 18035–48
[26] Kuramoto M, Kobayashi S, Akagi T, Tazawa K, Tanaka K, Saito T and Takeuchi T 2018 High-output-power and high-temperature operation of blue GaN-based vertical-cavity surface-emitting laser *Appl. Phys. Express* **11** 3
[27] Kumabe T, Kawasaki S, Watanabe H, Honda Y and Amano H 2023 Hole mobility limiting factors in dopant-free p-type distributed polarization-doped AlGaN *Appl. Phys. Lett.* **122** 252107
[28] Wang Y-C, Xia Y-B, Tian A-Q, Liu J-P, Geng X-B, Ying L-Y, Mei Y and Zhang B-P 2025 Performance enhancement of GaN-based VCSELs by composition-graded structures *Appl. Phys. Lett.* **127** 173305